Available online at www.sciencedirect.com
SCIENCE DIRECT®
PERGAMON
Polyhedron 22 (2003) 165–176
POLYHEDRON
www.elsevier.com/locate/poly

Structure and magnetism of trinuclear and tetranuclear mixed valent manganese clusters from dicyanonitrosomethanide derived ligands

David J. Price [a], Stuart R. Batten [a], Kevin J. Berry [b], Boujemaa Moubaraki [a], Keith S. Murray [a,*]

[a] School of Chemistry, Monash University, PO Box 23, Clayton, Vic. 3800, Australia
[b] Westernport Secondary College, Hastings, Vic. 3915, Australia

Received 25 July 2002; accepted 24 September 2002

Abstract

Two new mixed valent clusters of manganese have been synthesised in which the starting pseudochalcogenide ligand, dicyanonitrosomethanide, $(ONC(CN)_2^-$, (dcnm$^-$)) undergoes nucleophilic addition of methanol in complex **1** and water in complex **2** during coordination to the metal ions. Crystal structures show that complex **1** is a linear trinuclear Mn(II)Mn(III)Mn(II) compound, $[Mn_3(mcoe)_6]NO_3\cdot 2H_2O$, containing bridging oximate moieties from the chelating ligand methyl(2-cyano-2-hydroxyimino)ethanimidate ($[ONC(CN)C(NH)OCH_3]^-$, mcoe$^-$). Compound **2** has a planar rhomboidal (butterfly) arrangement of Mn(II)Mn(III)Mn(II)Mn(III) with the Mn(III) ions in 'body' positions bridged to the 'wingtip', seven coordinate Mn(II) ions by μ_3-oxo atoms and by the NO$^-$ oximato groups of the cyanoacetamidooximate chelating ligand, cao$^-$, $[ON{=}C(CN)CONH_2]^-$. **2** has the formula $(Me_4N)_2[Mn_4O_2(cao)_4(MeCN)_2(H_2O)_6](NO_3)_4\cdot 2H_2O$. There are hydrogen bonded cluster–cluster interactions in both compounds. Detailed susceptibility and magnetisation measurements on **1** and **2** reveal intra-cluster antiferromagnetic coupling with a total spin ground state at the crossover point of $S_T = 2$ and 1 for **1**, with other states very close in energy, and a rare sixfold degenerate set of S_T levels, 0,1,2,3,4,5, lying lowest in the case of **2**. In the latter case this is largely because of the large J_{13} (Mn(III)Mn(III)); body–body) value (-46.0 cm^{-1}) compared with the wing-body (Mn(II)Mn(III)) J_{12} value of -2.5 cm^{-1}. These coupling constants and S_T states are compared with those of other recent examples of planar rhomboidal mixed valent clusters, some of which show ferromagnetic J values and very large S_T ground states, with single-molecule magnetic behaviour exhibited in those cases. AC susceptibility studies show that complex **2** does not exhibit single-molecule magnetism behaviour.

Keywords: Dicyanonitrosomethanide derived oximate ligands; Mixed valent manganese clusters; Trinuclear; Tetranuclear; Magnetism; Crystal structures

1. Introduction

A great deal of recent research in polynuclear mixed valent manganese complexes has focussed on two main lines of enquiry. Firstly, in the bioinorganic area, many model complexes have been made to replicate the structure and function of manganese containing proteins and enzymes including, significantly, the water oxidation complex (WOC) in the Photosystem II (PSII) of green plants and cyanobacteria, which is responsible for the catalysis of the light driven oxidation of H_2O to O_2 [1–4]. Detailed spectroscopic, EXAFS, XANES and crystallographic studies have been made to probe the $Mn_4(Ca)$ μ-oxo cluster in the redox states S_0 to S_4 [5,6]. Secondly, in the field of nanomagnetic materials, some large high-spin manganese carboxylate clusters display magnetic properties previously only associated with nano-sized particles of magnetic metal oxides, that is, they can be magnetised and as such have been termed single-molecule magnets (SMMs). They also display unusual quantum mechanical effects in their single-crystal magnetisation hysteresis plots. The archetypal cluster, $[Mn(III/IV)_{12}O_{12}(OAc)_{16}(H_2O)_4]\cdot 2HOAc\cdot 4H_2O$ ('Mn_{12}-acetate') and its derivatives are the best and most comprehensively studied SMMs to date [7–13]. Other

* Corresponding author. Tel.: +61-3-9905-4512; fax: +61-3-9905-4597
E-mail address: keith.s.murray@sci.monash.edu.au (K.S. Murray).

0277-5387/02/$ - see front matter
PII: S0277-5387(02)01266-4

examples of SMMs include the family of complexes with the $[Mn(IV)Mn(III)_3O_3X]^{6+}$ core [14–16], where X^- is, for example, a halide, and other Mn_4 complexes such as $[Mn(III)_2Mn(II)_2]$ rhomboidal cores [17,18] as well as a number of Fe_4, Fe_8 and V_4 complexes [19–23]. More recently, a Ni_{12} wheel complex [24] and the first non-oxo-based SMM, the cyano bridged $MnMo_6(CN)_{18}$ cluster [25], have been isolated.

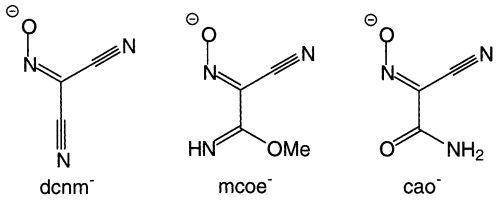

We present here two new mixed valent manganese complexes $[Mn_3(mcoe)_6]NO_3\cdot 2H_2O$ (**1**) and $(Me_4N)_2[Mn_4O_2(cao)_4(MeCN)_2(H_2O)_6](NO_3)_4\cdot 2H_2O$ (**2**), where $mcoe^-$ is methyl(2-cyano-2-hydroxyimino)ethanimidate ($[ONC(CN)C(NH)OCH_3]^-$) and cao^- is cyanoacetamidoximate ($[ON{=}C(CN)(CONH_2)]^-$). Their structures and magnetic properties are described.

This work arose from a combination of interests in Mn cluster chemistry and in 3D-molecular magnets based on pseudohalide and pseudochalcogenide bridges of cyano based ligands [26]. From such work we have recently reported a Mn_{16} cluster which displays aspects of SMM behaviour [27].

2. Experimental

$Mn(NO_3)_2\cdot 4H_2O$, methanol and acetonitrile were used as received. All reactions were performed under aerobic conditions. Me_4N(dcnm) was prepared by a metathesis reaction by adding an acetonitrile solution of Me_4NBr to a suspension of Ag(dcnm) in dichloromethane ($dcnm^-$ is $ONC(CN)_2^-$). AgBr was removed by filtration. The solvent was removed and the resulting yellow oil was recrystallised by vapour diffusion of diethyl ether into a solution in methanol (Yield 95%). Ag(dcnm) was synthesised according to the literature [28].

2.1. Synthesis of $[Mn_3(mcoe)_6]NO_3\cdot 2H_2O$ (1)

A methanolic solution (5 ml) of Me_4N(dcnm) (0.336 g, 2.0 mmol) was added to a methanolic solution (5 ml) of $Mn(NO_3)_2\cdot 4H_2O$ (0.251 g, 1.0 mmol). The resultant solution was an orange colour. After 1 week many red crystals were present in the deep red solution. The crystals had a hexagonal or half-hexagonal appearance and did not lose solvent in air. The solution was decanted. A fine light-brown solid, which coprecipitated with the crystals was removed by suspending it in methanol (the crystals were far less mobile, sinking rapidly) and decanting the suspension. This process was repeated several times until the methanol wash was free of the light-brown solid. The crystals were collected by filtration, washed with methanol and dried in air. Yield 0.17 g (50% based on total available Mn). An irregular shaped crystal was chosen for X-ray diffraction structural analysis. IR (Nujol, cm^{-1}), 3258s, 2221m, 1645s, 1434s, 1385m, 1356s, 1266s, 1192s, 1125s, 952w, 823w, 779m. *Anal*. Found: C, 29.5; H, 3.1; N, 24.8. Calc. for $C_{24}H_{28}N_{19}O_{17}Mn_3$: C, 28.3; H, 2.8; N, 26.1%. Powder XRD: The diffractogram of the bulk product matches that calculated from the crystal structure.

2.2. Synthesis of $(Me_4N)_2[Mn_4O_2(cao)_4(MeCN)_2(H_2O)_6](NO_3)_4\cdot 2H_2O$ (2)

Me4N(dcnm) (0.596 g, 3.54 mmol) was stirred in 10 ml of hot acetonitrile to dissolve. There remained a small amount of yellow residue. A solution of $Mn(NO_3)_2\cdot 4H_2O$ (0.889 g, 3.54 mmol) in acetonitrile (10 ml) was then added to this mixture, resulting in an instant colour change to deep red. Over a period of about 30 min of stirring the hot mixture changed to an orange colour. The mixture was then filtered several times to remove a fine brown precipitate (most likely manganese oxide), then covered and left to stand. After 4 days the solution was a red/brown colour with a small amount of fine brown precipitate mixed with many red/orange crystals. The fine brown precipitate was removed by suspending it in the solution (the crystals were far less mobile, the majority remaining attached to the glass of the vessel) and filtering the suspension. The filtrate was returned to the crystals, which were then filtered and washed with acetonitrile (Yield 50 mg, 4% based on total available Mn). IR (Nujol, cm^{-1}): 3390sbr, 2268vw, 2224s, 1682s, 1606s, 1470s, 1317s, 1224s, 1136s, 1041m, 950m, 831m, 708sh, 666sh. *Anal*. Found: C, 22.2; H, 3.0; N, 22.4. Calc. for $C_{24}H_{54}N_{20}O_{30}Mn_4$: C, 21.8; H, 4.1; N, 21.2%. Powder XRD: The diffractogram of the bulk product matches that calculated from the crystal structure.

2.3. X-ray crystallographic studies

Crystal data for **1** and **2** are summarised in Table 1. Data were collected using a Nonius KappaCCD diffractometer with graphite monochromated Mo-Kα radiation ($\lambda = 0.71073$ Å) Integration was carried out by the program DENZO-SMN [29], and data were corrected for Lorentz polarisation effects and for absorption using the program SCALEPACK [29]. Solutions were obtained by direct methods (SHELXS-97 [30]) followed by successive Fourier difference methods, and

Table 1
Summary of crystal data

	1	2
Formula	$C_{24}H_{28}Mn_3N_{19}O_{17}$	$C_{24}H_{54}Mn_4N_{20}O_{30}$
M	1019.47	1322.62
Crystal system	trigonal	monoclinic
Space group	$P\bar{3}1c$	$C2/c$
a (Å)	12.4720(2)	19.2163(3)
b (Å)	12.4720(2)	11.4283(2)
c (Å)	15.8114(4)	24.0215(2)
β (°)		90.916(1)
U (Å^3)	2129.97(7)	5274.7(2)
Z	2	4
T (K)	123(2)	123(2)
μ(Mo-Kα) (mm^{-1})	0.965	1.041
Crystal habit, colour	rhomboidal, red	rhomboidal, orange–red
Crystal size (mm)	0.15 × 0.125 × 0.1	0.2 × 0.2 × 0.1
Index ranges	$-16 \le h \le 16$, $-15 \le k \le 16$, $-21 \le l \le 21$	$-25 \le h \le 25$, $-15 \le k \le 15$, $-32 \le l \le 32$
Completeness to $2\theta = 55°$ (%)	99.9	99.2
Data collected	29 281	35 448
Unique data [R_{int}]	1775 [0.0908]	6442 [0.0619]
Observed reflections [$I > 2\sigma(I)$]	1390	4578
Parameters	106	292
Final R_1, wR_2 [$I > 2\sigma(I)$] (all data) [a]	0.0759, 0.2172, 0.0968, 0.2321	0.1134, 0.3314, 0.1502, 0.3563
Goodness-of-fit, S	1.141	1.097

[a] $R_1 = \Sigma||F_o|-|F_c||/\Sigma|F_o|$, $wR_2 = \{\Sigma[w(F_o^2-F_c^2)^2]/\Sigma[w(F_o^2)^2]\}^{1/2}$.

refined by full-matrix least-squares on F^2_{obs} (SHELXL-97 [30]).

For complex **1** all non-hydrogen atoms of the cation complex, the two waters of crystallisation and the nitrogen atom of the nitrate were refined anisotropically. The unique oxygen atom of the nitrate was found to be disordered over two positions. The two contributions (assigned equal quarter site occupancies) were refined isotropically. The imidate proton was located in the difference Fourier map and was subsequently refined isotropically. The methoxy protons of the mcoe$^-$ ligand were included at calculated positions with U values 1.5 times the U_{eq} of the carbon atom. Two regions of electron density not connected to each other were assigned as two water molecules. Table 2 contains selected distances and angles.

For complex **2** all non-hydrogen atoms of the cluster were refined anisotropically. Due to significant disorder that was difficult to model the non-hydrogen atoms of the tetramethylammonium and nitrate counter ions were refined isotropically and no hydrogen atoms were assigned. A region of residual electron density was assigned as a water molecule disordered over two positions (O(600) and O(601)). Hydrogen atoms on the coordinating acetonitrile molecules and the amine groups of the cao$^-$ ligands were assigned to calculated positions with U values 1.5 times (for methyl protons) and 1.2 times (for amine protons) the U_{eq} of the attached atom, whereas those on the coordinating water molecules were not located. As can be seen in Table 1 the final R-value was relatively high. The crystals were quite small and weakly diffracting and many were tried with poorer quality diffraction. A number of solutions were obtained for different crystals, the best giving the refined structure presented here. Despite the extreme disorder in the counter ions and in a water molecule the cluster itself is well refined. Table 3 contains selected distances and angles.

Table 2
Selected bond distances (Å) and angles (°) of **1**

Bond lengths			
Mn(1)–O(1)	2.169(3)	Mn(1)···Mn(2)	3.9177(9)
Mn(2)–N(2)	2.324(3)	Mn(2)–N(9)	2.189(4)
O(1)–N(2)	1.301(4)	C(3)–C(6)	1.490(5)
N(2)–C(3)	1.303(5)	C(6)–N(9)	1.250(6)
C(3)–C(4)	1.410(6)	C(6)–O(7)	1.338(5)
C(4)–N(5)	1.14(1)	O(7)–C(8)	1.462(6)
Bond angles			
O(1)–Mn(1)–O(1^{i})	90.7(1)	N(2)–Mn(2)–N(9)	72.2(1)
O(1^{i})–Mn(1)–O(1^{ii})	82.6(1)	N(9)–Mn(2)–N(9^{ii})	92.73(14)
O(1)–Mn(1)–O(1^{ii})	93.5(9)	N(2)–Mn(2)–N(2^{ii})	85.33(12)
O(1)–Mn(1)–O(1^{iii})	174.5(1)	N(2)–Mn(2)–N(9^{ii})	138.15(13)
		N(2^{ii})–Mn(2)–N(9)	125.91(12)
Hydrogen bonding			
N(9)–H(9)	1.00(7)		
H(9)···O(110)	2.00(7)	H(9)···O(111)	2.02(7)
N(9)···O(110)	2.94(3)	N(9)···O(111)	2.90(2)
N(9)–H(9)···O(110)	156(5)	N(9)–H(9)···O(111)	147(5)

Symmetry transformations (i) $-x+y$, y, $-z+3/2$; (ii) $-y+1$, $x-y+1$, z; (iii) $-y+1$, $-x+1$, $-z+3/2$.

2.4. Magnetic measurements

Magnetic measurements were carried out as described previously [26] using a Quantum Design MPMS 5 Squid magnetometer for DC magnetisation measurements and a PPMS instrument for AC susceptibility measurements. Since Mn(III) complexes display torquing at low temperatures [31], the powder samples were dispersed in Vaseline.

3. Results and discussion

3.1. Synthesis and characterisation

Complex **1** crystallises out of a solution of $Mn(NO_3)_2 \cdot 4H_2O$ and Me_4N(dcnm) (1:2 molar ratio) in methanol. Complex **2** crystallised out of a solution of equimolar

Table 3
Selected bond distances (Å) and angles (°) of **2**

Bond lengths			
Mn(1)–O(1)	2.077(5)	Mn(2)–O(1)	1.844(5)
Mn(1)–N(3)	1.924(2)	Mn(2)–O(1^{i})	1.837(5)
Mn(1)–O(9)	2.241(6)	Mn(2)–O(2)	2.003(5)
Mn(1)–N(11)	2.425(6)	Mn(2)–O(10^{i})	1.993(5)
Mn(1)–O(17)	2.226(6)	Mn(2)–O(20)	2.296(8)
Mn(1)–O(18)	2.192(7)	Mn(2)–N(21)	2.372(9)
Mn(1)–O(19)	2.180(9)	Mn(2)···Mn(2^{i})	2.773(2)
Mn(1)···Mn(2)	3.546(2)		
Bond angles			
O(1)–Mn(1)–O(19)	93.7(3)	O(17)–Mn(1)–N(3)	142.9(2)
O(1)–Mn(1)–O(18)	87.3(2)	O(9)–Mn(1)–N(3)	68.4(2)
O(19)–Mn(1)–O(18)	176.3(3)	O(1)–Mn(2)–O(1^{i})	82.3(2)
O(1)–Mn(1)–O(17)	142.3(2)	O(1^{i})–Mn(2)–O(10^{i})	93.7(2)
O(19)–Mn(1)–O(17)	90.0(4)	O(1)–Mn(2)–O(10^{i})	175.9(2)
O(18)–Mn(1)–O(17)	91.4(3)	O(1^{i})–Mn(2)–O(2)	176.5(2)
O(1)–Mn(1)–O(9)	143.1(2)	O(1)–Mn(2)–O(2)	94.6(2)
O(19)–Mn(1)–O(9)	86.7(3)	O(2)–Mn(2)–O(10^{i})	89.4(2)
O(18)–Mn(1)–O(9)	90.3(3)	O(1^{i})–Mn(2)–O(20)	95.9(3)
O(17)–Mn(1)–O(9)	74.6(2)	O(1)–Mn(2)–O(20)	93.8(3)
O(1)–Mn(1)–N(11)	73.9(2)	O(10^{i})–Mn(2)–O(20)	87.0(3)
O(19)–Mn(1)–N(11)	90.3(3)	O(2}–Mn(2)–O(20)	82.5(3)
O(18)–Mn(1)–N(11)	93.4(2)	O(1^{i})–Mn(2)–N(21)	94.9(3)
O(17)–Mn(1)–N(11)	68.5(2)	O(1)–Mn(2)–N(21)	93.4(3)
O(9)–Mn(1)–N(11)	143.0(2)	O(10^{i})–Mn(2)–N(21)	86.4(3)
O(1)–Mn(2)–N(3)	74.6(2)	O(2)–Mn(2)–N(21)	87.0(3)
O(19)–Mn(1)–N(3)	90.8(3)	O(20)–Mn(2)–N(21)	167.7(3)
O(18)–Mn(1)–N(3)	86.0(2)	Mn(2)–O(1)–Mn(2^{i})	97.7(2)
Hydrogen bonding			
O(19)···O(52^{iv})	3.07(2)	O(20)···O(43)	2.82(2)
O(19)···O(53)	2.63(2)	N(8)···N(6^{iii})	3.00(1)
O(18)···O(43^{i})	2.86(2)	N(16)···N(14^{v})	3.03(1)
O(18)···O(600^{ii})	2.49(5)	N(8)···O(43^{ii})	2.90(2)
O(600)···O(41)	2.40(5)	N(16)···O(600^{iv})	2.90(4)
O(601)···O(41)	2.34(4)	N(16)···O(601^{iv})	2.67(3)
O(52^{iv})···O(19)···O(53)	124.9(7)	N(8)–H(8B)···N(6^{iii})	149.4
N(8)–H(8A)···O(43^{ii})	175.9	N(16)–H(16B)···N(14^{v})	152.9

Symmetry transformations (i) $-x+1/2$, $-y+3/2$, $-z+1$; (ii) $x-1/2$, $y-1/2$, z; (iii) $-x$, y, $3/2-z$; (iv) $-x$, $2-y$, $1-z$; (v) $-x$, y, $3/2-z$.

amounts of $Mn(NO_3)_2{\cdot}4H_2O$ and Me_4N(dcnm) in hot acetonitrile. A brown solid, which from IR spectroscopy is likely to be MnO_2, is formed in relatively large quantities at the same time as some of the Mn(II) is oxidised to Mn(III), which is then included in the tetranuclear cluster. This solid can be filtered off progressively during the course of the reaction. In latter stages, the majority of the product is **2** and can be relatively successfully separated from remaining MnO_2 powder. The yield of **2** was very low but quite reproducible.

Infrared spectroscopy of complex **1** shows absorbances at 2221 and 1645 cm^{-1} corresponding to the ν(C≡N) and ν(C=N) vibrations, respectively, from the $mcoe^-$ ligand. Likewise for complex **2** absorbances at 2224 and 1682 cm^{-1} correspond to the ν(C≡N) and ν(C=O) vibrations of the cao^- ligand.

The pseudochalcogenide ligand dicyanonitrosomethanide ($ONC(CN)_2^-$, $dcnm^-$) undergoes nucleophilic addition of solvent (methanol and water for complexes **1** and **2**, respectively) in the coordination sphere of the metal to form the chelating ligands, methyl(2-cyano-2-hydroxyimino)ethanimidate ($[ONC(CN)C(NH)OCH_3]^-$, $mcoe^-$) for **1** and cyanoacetamidoximate ($[ON=C(CN)(CONH_2)]^-$, cao^-) for **2**. The nucleophilic addition of solvent to $dcnm^-$ has been reported by Hvastijová et al. for Co(II), Ni(II), Cu(II) and Pd(II) complexes [32–36]. The protonated form of the ligand, caoH, has been synthesised recently by refluxing the filtrate formed from the reaction of Ag(dcnm) and NH_4Cl in water [37]. Compounds **1** and **2** are the first examples of complexes in which the $mcoe^-$ and cao^- ligands occupy bridging as well as chelating coordination modes. The oxidation of Mn(II) to Mn(III) and Mn(IV) (MnO_2) in these aerobic reactions is not unexpected and the formation of Mn(II)OMn(III) bridges in **2** under these conditions is common.

3.2. Crystal structures

3.2.1. $[Mn_3(mcoe)_6]NO_3{\cdot}2H_2O$ (**1**)

Complex **1** crystallises in the trigonal space group $P\bar{3}1c$. The cation is a linear trinuclear complex (Fig. 1) with the three manganese ions lying along a threefold axis and the central manganese atom situated on an inversion centre. Thus the asymmetric unit contains 1/6 of the formula unit. The cation contains two symmetry related terminal six-coordinate manganese(II) ions chelated by the N-donor atoms of the imidate and oxime groups of three $mcoe^-$ ligands in a trigonal prismatic environment (Mn(2)–N(9) = 2.189(4), Mn(2)–N(2) = 2.324(3) Å and N(2)–Mn(2)–N(9) = 72.2(1)°). The two terminal manganese(II) ions are bridged to the central manganese(III) by the oxime groups of the six $mcoe^-$ ligands, providing an entirely O-donor atom coordination environment in a distorted octahedral fashion (Mn(l)–O(l) = 2.169(3) Å).

The oxidation states are assigned on the basis of charge balance and on consideration of bond lengths. The two terminal manganese ions are assigned Mn(II) due to the longer average bond length (2.257(7) Å) compared with the bond length for the central manganese ion, which was assigned as Mn(III). It would be expected that the central Mn(III) ion would show Jahn–Teller distortion, having d^4 configuration in a near-octahedral environment. However, in this case, there is only one unique Mn–O bond length.

This complex strongly resembles the linear trinuclear mixed oxidation state manganese complexes $[(Me_3\text{-tacn})Mn(III)\{(\mu\text{-niox})_3M(II)\}Mn(III)(Me_3\text{-tacn})](ClO_4)_2$, (M(II) = Mn, Cu and Zn; Me_3-tacn = 1,4,7-trimethyl-1,4,7-triazacyclononane; H_2niox = cyclohexane-1,2-dione) published by Birkelbach et al. [38,39]. In

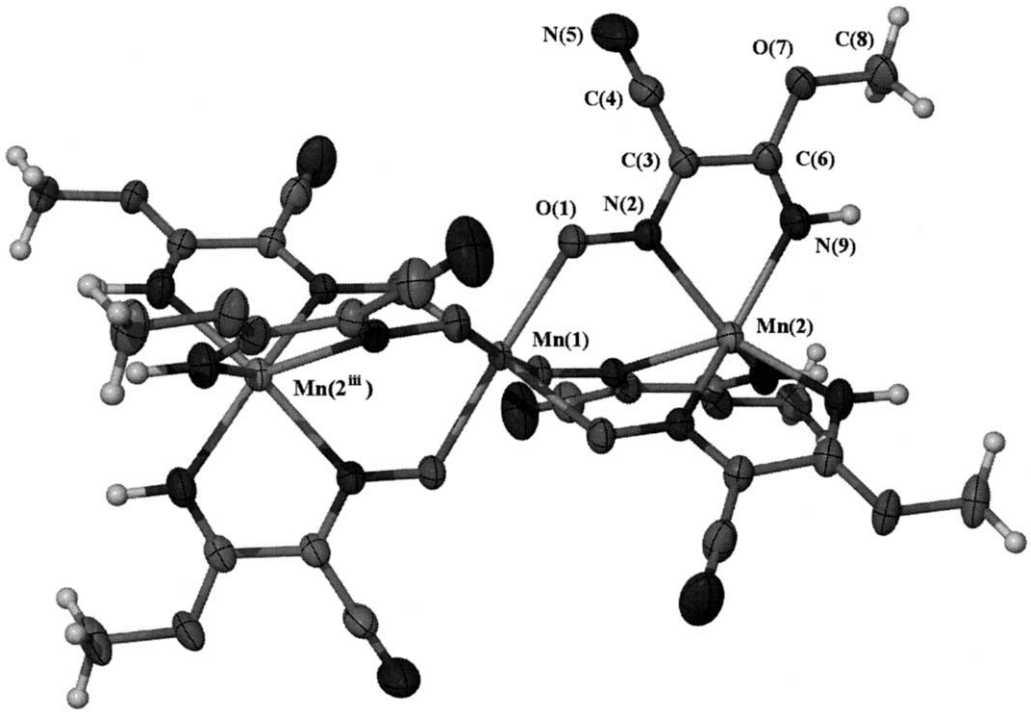

Fig. 1. Crystal structure of $[Mn_3(mcoe)_6]NO_3\cdot 2H_2O$ (**1**) with atom labelling scheme (thermal ellipsoids shown at 50% probability). NO_3^- and lattice waters omitted.

contrast to **1**, these complexes consist of a central M(II) ion chelated by three $niox^{2-}$ ligands in a trigonal prismatic environment with an entirely N-donor atom coordination sphere, and are then bridged to the two terminal Mn(III) ions by the oxime groups of the $niox^{2-}$ ligands. The terminal Mn(III) ions are in turn capped by Me_3-tacn and thus possess a distorted octahedral N_3O_3 coordination environment. Other linear Mn(III) Mn(II)Mn(III) examples are known [40].

Each cation in **1** is linked to its neighbour along the *c*-axis via hydrogen bonding between the cation imidate protons and the nitrate counter ion (N(9)···O(111) = 2.90(1) Å) (Fig. 2), which is disordered over two positions related by a 48.8(1)° rotation about the nitrogen atom. This disorder in the nitrate oxygen may be due to the hydrogen bonding between the three imidate protons each on adjacent complexes that are staggered 60° with respect to each other.

3.2.2. $(Me_4N)_2[Mn_4O_2(cao)_4(MeCN)_2(H_2O)_6](NO_3)_4\cdot 2H_2O$ (**2**)

Complex **2** crystallises in the monoclinic space group *C*2/*c*, with the tetranuclear manganese cluster lying on an inversion centre. Table 3 contains selected bond distances and angles for **2**. Fig. 3 shows the cluster and the atom labelling scheme. The asymmetric unit contains half of the cluster, one tetramethylammonium and two nitrate counter ions and one lattice water. The cluster contains a $[Mn_4(\mu_3\text{-}O)_2]^{6+}$ core (2Mn(II), 2Mn(III)) in which the four Mn atoms lie in a diamond shaped plane with Mn(l)···Mn(2) = 3.546(2) Å being considerably longer than Mn(2)···Mn(2^i) = 2.773(2) Å. This is due to the latter pair being bridged by two μ_3-O^{2-} atoms (Mn(2)–O(1) = 1.844(3)(2) Å and Mn(2^i)–O(1) = 1.837(5) Å), whereas the former pair are bridged by the two atom N–O moiety of the cao^- ligand (Mn(l)–N(3) = 2.436(6) Å and O(2)–Mn(2) = 2.003(5)

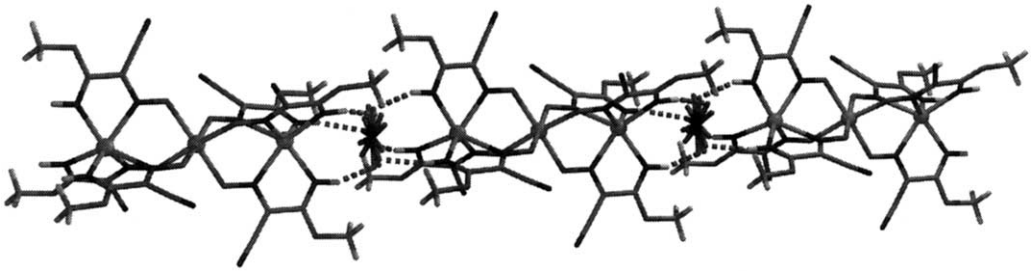

Fig. 2. Hydrogen bonding of $[Mn_3(mcoe)_6]^+$ cations alternating with disordered nitrate anions (H-bonds dashed, methyl protons omitted for clarity).

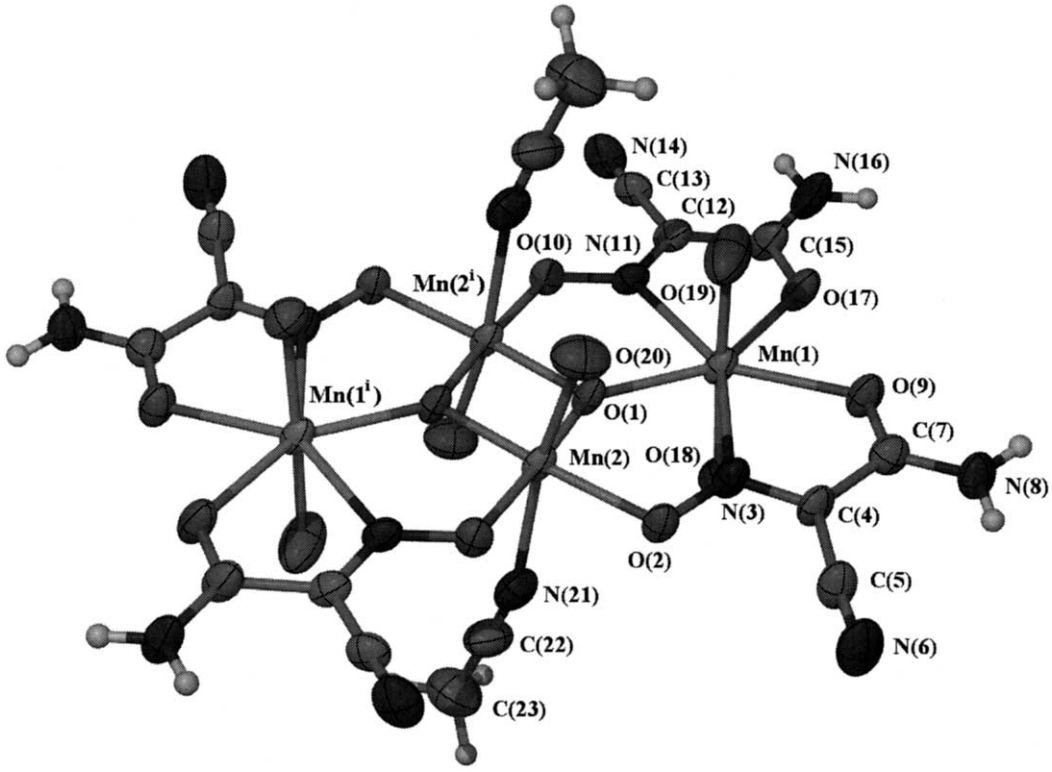

Fig. 3. Crystal structure of **2** with atom labelling scheme (thermal ellipsoids shown at 50% probability). Hydrogen atoms, counter ions and lattice waters omitted.

Å) and a single μ_3-O^{2-} atom (Mn(1)–O(1) = 2.077(5) Å). The μ_3-O^{2-} atom lies 0.190(6) Å out of the plane defined by the four manganese atoms. On the periphery of the $[Mn_4(\mu_3\text{-}O)_2]^{6+}$ core are four chelating cao^- ligands (two of which are unique) which lie roughly coplanar with the core. In the axial positions of the metal coordination spheres are six terminal water molecules, two each on Mn(1) and Mn(1^i) and one each on Mn(2) and Mn(2^i), and two terminal acetonitrile ligands, one each on Mn(2) and Mn(2^i).

The two Mn(II) atoms (Mn(1) and Mn(1^i) are thus seven coordinate in an approximate pentagonal bipyramidal arrangement. The carbonyl oxygens (O(9) and O(17)) and oxime nitrogens (N(3) and N(11)) of two cao^- ligands and one μ_3-O^{2-} ion (O(1)) make up the pentagonal plane of the bipyramid, whereas the apices are filled by the two axial waters (O(18) and O(19)). The five angles around the plane are 68.4(2)°, 68.5(2)°, 73.9(2)°, 74.6(2)° and 74.6(2)°. The sum of these angles being 360° attests to the planarity of the coordination environment. The non-coordinating nitrile groups of the two cao^- ligands chelating each Mn(II) ion are bent slightly away from the plane of the $[Mn_4(\mu_3\text{-}O)_2]^{6+}$ core. Mn(2) and Mn(2^i) were assigned as Mn(III) ions on the basis of the significant Jahn–Teller elongation in the direction of the axial water and acetonitrile ligands (Mn(2)–O(20) = 2.296(8) Å and Mn(2)–N(21) = 2.372(9) Å, where the average equatorial bond distance = 1.92 Å), as expected for a high-spin Mn(III) (d^4) in near-octahedral geometry.

A complex network of hydrogen bonding exists between the clusters and the intercalated water and nitrate anions. Inspection of the cluster shows that there are several sites capable of hydrogen bonding, and the cluster packing is determined by the hydrogen bonding interactions. Broadly speaking there are two intersecting hydrogen bonding networks. Firstly, a sheet in the *ab*-plane is formed by hydrogen bonding interactions between adjacent clusters (perpendicular to the plane of the clusters) via the terminal waters, the nitrate anions and the intercalated water molecule. Secondly, another sheet network is formed in the *ac*-plane by hydrogen bonding between the terminal amine and the nitrile groups of the cao^- ligand on adjacent clusters. The tetramethylammonium cations pack between the sheets in the *ab*-plane.

The network in the *ab*-plane involves multiple hydrogen bonding interactions and can be broken down into two types of intersecting chains. The terminal water oxygen atom O(19) on Mn(2) hydrogen bonds to two symmetry related nitrate anions (O(19)···O(52^{iv}) = 3.07(2), O(19)···O(53) = 2.63(2) Å and O(52^{iv})···O(19)···O(53) = 124.9(7)°) which in turn both hydrogen bond to a symmetry related O(19) on an adjacent cluster. The pattern thus formed is a stepped chain of clusters (Fig. 4(a)). In addition another chain in

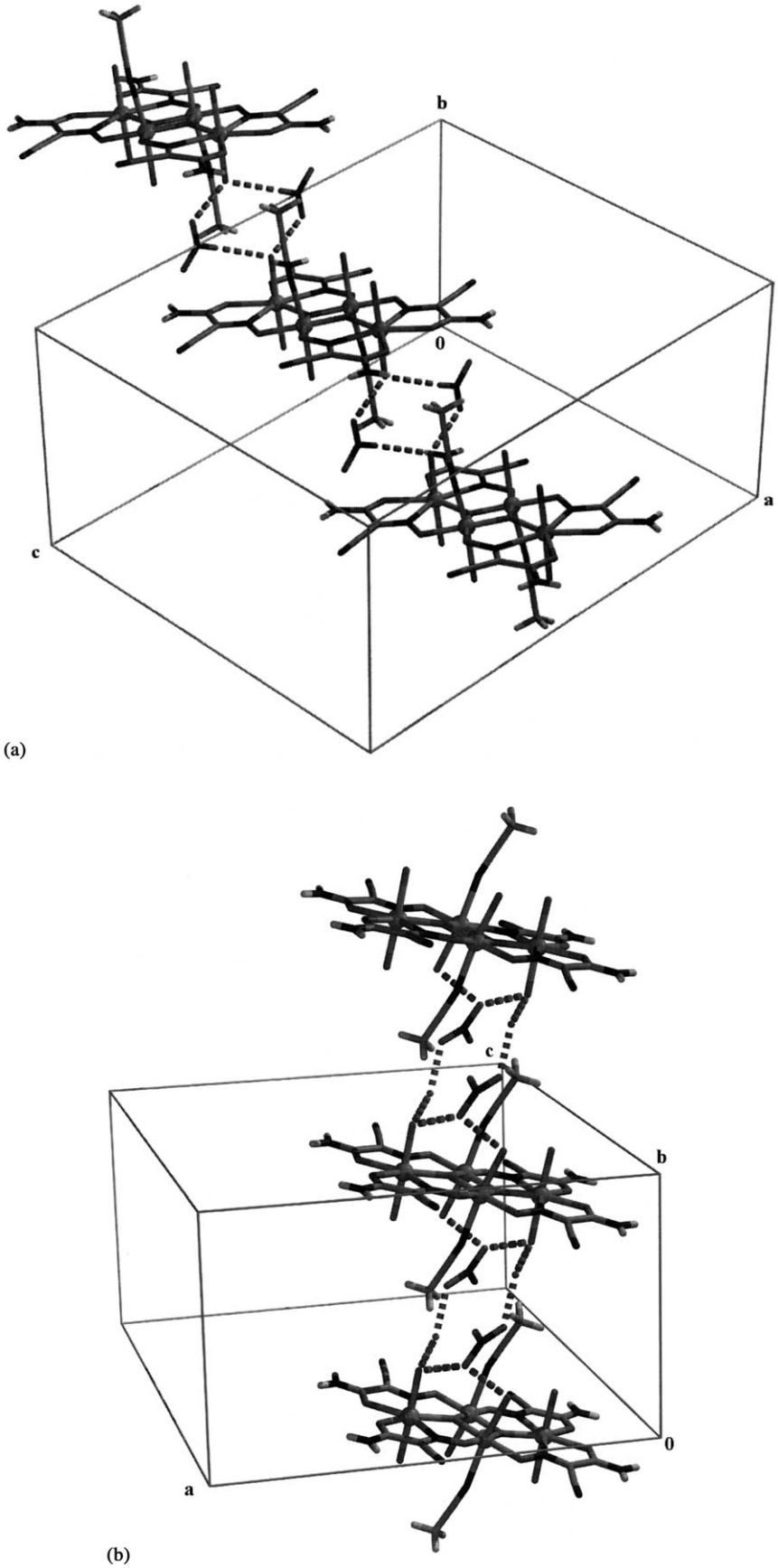

Fig. 4. (a) The stepped chain section of the hydrogen bond network (dashed) of **2** in the *ab*-plane. (b) Second part of the hydrogen bonded network (dashed) of **2** in the *ab*-plane. (c) Hydrogen bonded network (dashed) of **2** in the *ac*-plane.

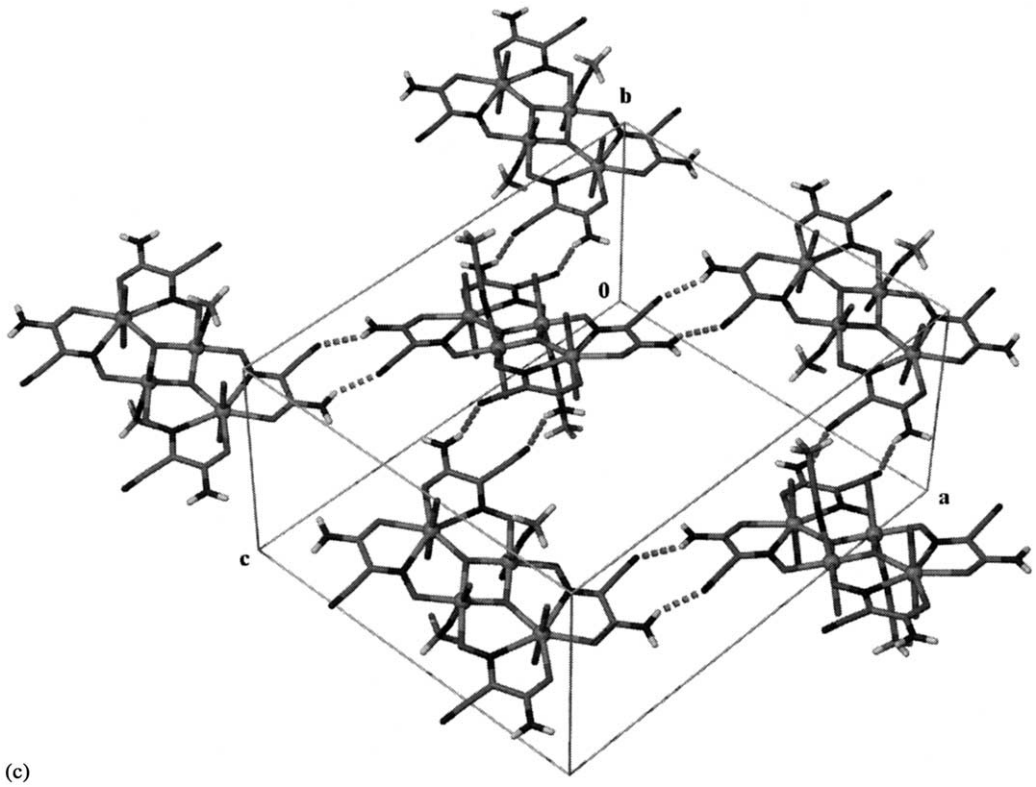

Fig. 4 (*Continued*)

this plane exists that involves hydrogen bonding from the water O(18) coordinated to Mn(2) to both a nitrate anion (O(18)···O(43^{i}) = 2.86(2) Å) and a disordered water (average O···O distance = 2.9(1) Å) which in turn hydrogen bond to their symmetry related partners (nitrate-water average O···O distance = 2.37(9) Å), which then also hydrogen bond to O(18) on the adjacent cluster (Fig. 4(b)). The water coordinated to the central Mn(1) also hydrogen bonds to the nearby nitrate anion that is also hydrogen bonded to O(18) (O(20)···O(43) = 2.82(2) Å).

The sheet in the *ac*-plane (Fig. 4(c)) is set up by the terminal amines and nitriles of the two unique cao^{-} ligands, so that the amine on one cluster hydrogen bonds to the nitrile on the adjacent cluster (N(8)···N(6^{iii}) = 3.00(1) Å, N(8)–H(8B)···N(6^{iii}) = 149.4° and N(16)···N(14^{v}) = 3.03(1) Å, N(16)–H(16B)···N(14^{v}) = 152.9°). All hydrogen bonds in the plane are directed parallel to the *c*-axis direction. The topology of this sheet is (4,4). Viewed parallel to the *c*-axis direction the sheets undulate due to the planes of adjacent clusters in the *a*-axis direction being on an angle of 31.48(3)° to each other (mean planes of Mn atoms). The terminal amine on one of the cao^{-} ligands also hydrogen bonds to a nearby nitrate anion (N(8)···O(43^{ii}) = 2.90(2) Å, N(8)–H(8A)···O(43^{ii}) = 175.9°) and correspondingly the other amine hydrogen bonds to the disordered lattice water molecule with an average distance of 2.79(7) Å. Thus the amine groups also participate in the hydrogen bonded network in the *ab*-plane.

3.3. Magnetism

3.3.1. $[Mn_3(mcoe)_6]NO_3\cdot 2H_2O$ (**1**)

In Fig. 5(a) it can be seen that the magnetic moment, per Mn_3, decreases a little from 9.5μ_B at 300 K to ~9μ_B at ~100 K, then more rapidly to reach a shoulder value of 5.5μ_B at 5 K before reaching 4.7μ_B at 2 K. The uncoupled ($g = 2.0$) value for $S_1 = 5/2$, $S_2 = 4/2$, $S_3 = 5/2$ is 9.70μ_B and thus very weak antiferromagnetic coupling is occurring. The 2 K value is suggestive of a $S_T = 2$ coupled ground state but, since J values are small, there will be many M_S energy levels populated because of their close spacing of a few cm^{-1}. The crossover of relevant S_T levels occur at the following α values where $\alpha = J_{13}/J_{12}$ and J_{12} is negative:

$S_T = 3 \quad \alpha < 0.4$

$S_T = 2 \quad 0.4 < \alpha < 0.5$

$S_T = 1 \quad \alpha > 0.5$

The spin Hamiltonian employed is that commonly used for a linear trimer:

$$\boldsymbol{H} = -2J_{12}(\boldsymbol{S}_1 \cdot \boldsymbol{S}_2 + \boldsymbol{S}_2 \cdot \boldsymbol{S}_3) - 2J_{13}\boldsymbol{S}_1 \cdot \boldsymbol{S}_3$$

The field-dependent thermodynamic form of suscept-

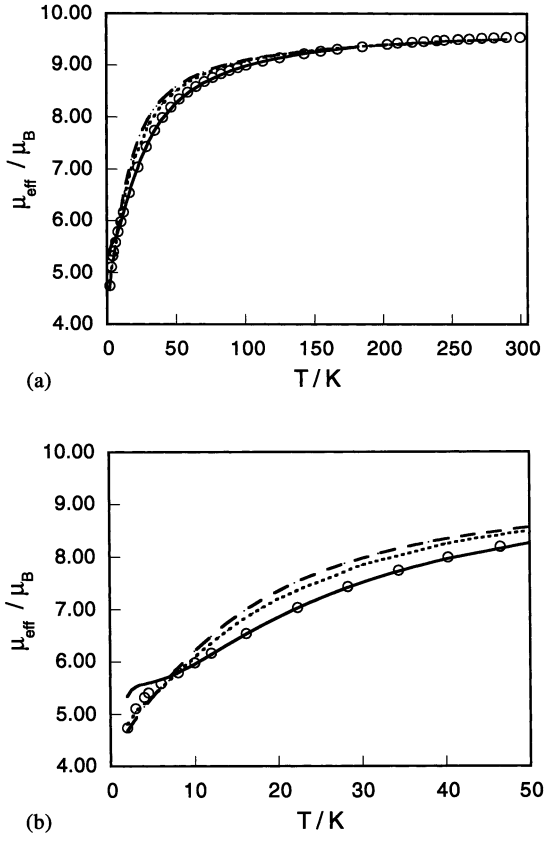

Fig. 5. (a) Plot of observed μ_{eff} data for complex **1** (2–300 K, $H = 1$ T). Calculated lines are obtained using the parameter sets (a) to (c) (see text) are given, (a) - - - -, (b) ·····, (c) —. (b) Plot of observed μ_{eff} data for complex **1** in region 2–50 K with calculated lines for parameter sets (a) - - - -, (b) ·····, (c) — (see text).

ibility was employed [17,18,41]. Wide ranges of parameter values were explored in trying to fit the whole susceptibility data between 2–300 K. The region 12–120 K was the hardest to reproduce. Using χ_{TIP} of 300×10^{-6} cm^3 mol^{-1}, the following three sets gave quite good fits:

a) $g = 1.99$, $J_{12} = -1.02$ cm^{-1}, $J_{13} = -0.53$ cm^{-1}, $\alpha = 0.52$, $S_T = 1$ ground;
b) $g = 2.00$, $J_{12} = -1.16$ cm^{-1}, $J_{13} = -0.58$ cm^{-1}, $\alpha = 0.50$, $S_T = 1$ or 2 ground;
c) $g = 2.02$, $J_{12} = -1.59$ cm^{-1}, $J_{13} = -0.67$ cm^{-1}, $\alpha = 0.42$, $S_T = 2$ ground.

Fit (c) was better than (a) and (b) between 10–120 K but worse below 6 K (Fig. 5(b)). It is possible that the small discrepancy below 6 K arises through trimer–trimer interactions. Variable field magnetisation isotherms ($T = 2$–20 K, $H = 0$–5 T) were measured to help to identify the S_T ground state. Saturation in M is not complete even at 2 K and 5 T.

Calculation of the M versus H plots at 2 K and 0–5 T using the parameter sets (a) to (c) gave the worst agreement for set (c) with calculated M values being

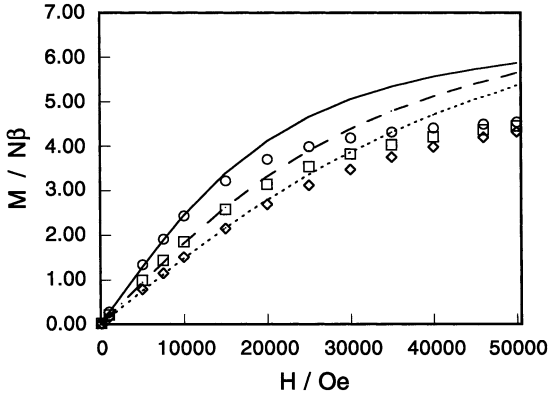

Fig. 6. Plots of isothermal (2, 3, 4 K) magnetisation data vs. field, H, for complex **1**. Calculated lines (— 2 K, ------ 3 K, ·····4 K) use parameter set (a) given in the text and the spin Hamiltonian given, which does not include zero-field splitting terms.

bigger than observed at all temperature and field combinations. Sets (a) and (b) gave similar calculated values and showed good agreement for the three temperatures with fields between 0–1.5 T but with calculated M values greater than those observed above 1.5 T (Fig. 6). It is interesting to note that the 2 K/5 T calculated values of M are significantly greater than $4N\beta$ anticipated for $S_T = 2$ lowest in energy because of thermal population of the $S_T = 3$ and $S_T = 1$ Zeeman levels close by. In summary, the α value appears to be close to 0.5, the crossover point of $S_T = 1$ and 2. The discrepancies between observed and calculated M values above fields of 1.5 T are most likely because of zero-field splitting effects combined with Zeeman effects from closely spaced S_T levels. There is not an isolated S_T ground state for complex **1** and so further attempts to calculate D values have not been made. Plots of observed M versus H/T (K), either isothermal (2–20 K) or isofield [17,18], show non-superposition of the lines and are thus indicative of zero-field splitting effects. Weak trimer–trimer effects may also play a minor part in the higher field regimes.

The J_{12} value for **1** of ~ -1 cm^{-1}, which results from Mn(III)–O–N(R)–Mn(II) superexchange pathways can be compared with the related nioximato- and dimethylglyoximato-bridging in the work of Birkelbach et al. [38,39] in which J_{12} was $+4.7$ cm^{-1} (with $J_{13} = -3.0$ cm^{-1}). The difference in sign of J_{12} results from the net effects of the ferromagnetic and antiferromagnetic contributions to J_{12} which, in turn, will be influenced by subtle coordination differences on the Mn(III) and Mn(II) centres and, to a lesser degree by the terminal binding groups. These structural differences have been described above in Section 3.2.1.

3.3.2. $(Me_4N)_2[Mn_4O_2(cao)_4(MeCN)_2(H_2O)_6](NO_3)_4{\cdot}2H_2O$ (**2**)

Two fresh samples were measured and very similar μ_{eff} (per Mn_4) data were obtained when measured in a

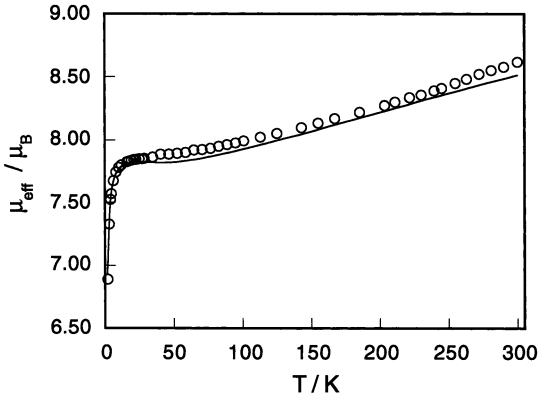

Fig. 7. Plot of observed μ_{eff} data for complex **2** (2–300 K, $H = 1$ T). Best-fit calculated line obtained using the parameter set given in the text.

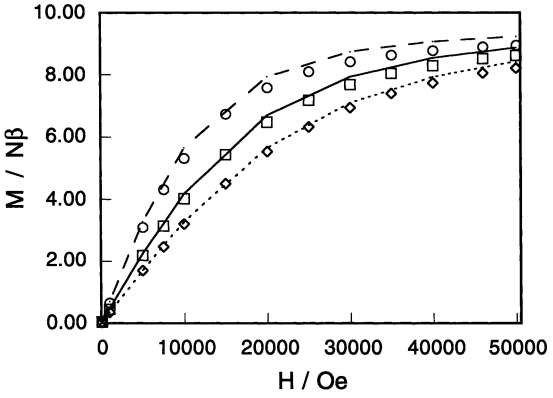

Fig. 8. Plots of isothermal (2, 3, 4 K) magnetisation data vs. field, H, for complex **2**. Calculated lines (------ 2 K, — 3 K, ····· 4 K) use the parameter set given in the text and in Table 4. The kinks in the calculated curves reflect the number of calculated points used in the plotting routine.

field of 1 T and dispersed in Vaseline to prevent torquing. The moment decreases, gradually, from $8.65\mu_B$ at 300 K to reach a plateau value of $\sim 7.8\mu_B$ between 50–10 K, then more rapidly reaching $6.85\mu_B$ at 2 K and still decreasing (Fig. 7). The spin-only value for two Mn(III) ($S = 2$) plus two Mn(II) ($S = 5/2$) of $\mu = 10.86\mu_B$ is bigger than the observed value at 300 K. Thus antiferromagnetic coupling is occurring. The 'butterfly' tetranuclear arrangement of spins, with two Mn(III)(2,2′) in the body positions and two Mn(II)(1,1′)) at the wingtips was employed in the ($-2JS_1 \cdot S_2$) spin Hamiltonian [17,18,41] with the spin centres numbered as follows.

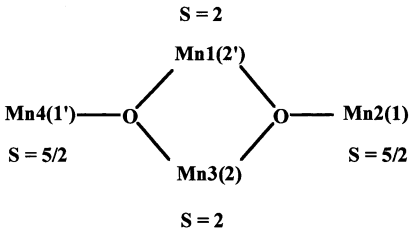

The Kambe vector coupling approach has been described for this spin combination [17,18,41]. There are 110 possible spin states with S_T, the total spin of the cluster, varying from 0 to 9. We use the field-dependent thermodynamic form of susceptibility, in combination with matrix diagonalisation methods, to fit the susceptibility data.

The best-fit to the data is obtained for the parameter set $g = 1.88$, $J_{12} = -2.5$ cm^{-1}, $J_{13} = -46.0$ cm^{-1}, $\alpha = J_{13}/J_{12} = 18.4$, $J_{24} = 0$. These parameters also give good agreement with the 2, 3 and 4 T magnetisation isotherms (Fig. 8). Interestingly, the ground state under these conditions, viz $\alpha > 6$, J_{12} and J_{13} negative and with J_{13} large, is made up of the six degenerate levels $S_T = 0$, 1,2, 3, 4, 5 and they correspond to $S_{13} = 0$. Introduction of a tiny J_{24} value of -0.02 cm^{-1} has only a minimal effect on the quality of fit. Larger J_{24} values such as ± 0.1 cm^{-1}, which correspond to splitting up of the six S_T levels, lead to much poorer fits. Thus, we do not have an isolated S_T ground level in **2** and plots of M versus H/temperature, much used by Hendrickson and Christou [17,18] to show zero-field splitting of isolated ground states, yield isofield lines all superimposed on each other thus indicating a lack of zero-field splitting.

Table 4
Comparison of J values (cm^{-1}) and ground spin states for $Mn(II)_2Mn(III)_2$ planar rhomboidal cores where $Mn_1 = Mn_3 = Mn(III)$ at body sites

Cluster	J_{12}	J_{13}	$\alpha = J_{13}/J_{12}$	g	Ground S_T	References
2	−2.5	−46.0	18.4	1.88	0–5 [d]	[e]
$Mn_4O_2(O_2CCH_3)_6(bipy)_2$ [a]	−1.97	−3.12	1.59	1.70	2	[42]
$Mn_4O_2(O_2CCPh_3)_6(OEt_2)_2$	−1.50	−2.80	1.89	1.47	2	[43]
$[Mn_4(O_2CCH_3)_2(pdmH)_6](ClO_4)_2$ [b]	+0.20	+4.05	20.4	1.84	8 ± 1	[17]
$[Mn_4(O_2CCH_3)_2(pdmH)_6]\cdot 2.5H_2O$	+0.55	+4.35	7.94	1.89	9	[17]
$[Mn_4(hmp)_6Br_2(H_2O)_2]Br_2\cdot 4H_2O$ [c]	+0.47	+4.42	9.43	1.94	9	[18]

[a] bipy = 2,2′-bipyridine.
[b] $pdmH^-$ = monoanion of pyridine-2,6-dimethanol.
[c] hmp^- = anion of 2-hydroxymethylpyridine.
[d] Six degenerate levels.
[e] This work.

The J values and ground S_T states for other recently reported $Mn(II)_2Mn(III)_2$ planar-rhomboidal compounds are compared with those of **2** in Table 4. The first three compounds have μ_3-oxo bridges and J_{13} (body–body Mn(III)···Mn(III)) is much more negative for complex **2** than for the others. The μ_3-phenoxo bridged compounds containing $pdmH^-$ and hmp^- ligands show ferromagnetic J_{12} and J_{13} values possibly because of the nature of the orbital overlap involving the phenoxo oxygen. These J values lead to large S_T ground state values with negative zero-field splitting. Such features are prerequisites for single-molecule magnetic (SMM) behaviour and this was confirmed for these molecules by observing frequency dependent out of-phase components χ''_M. We would predict that complex **2** should not exhibit SMM behaviour because of a lack of zero-field splitting. Measurements of the AC χ''_M values versus temperature (2−10 K; oscillation frequencies 10, 50, 100, 250, 500, 1500 Hz; AC field amplitude 3.5 Oe) showed no maximum in this temperature range and thus **2** does not display SMM behaviour.

4. Supplementary material

Crystallographic data for the structural analysis have been deposited with the Cambridge Crystallographic Data Centre, CCDC Nos. 190372 and 190373. Copies of this information may be obtained free of charge from the Director, CCDC, 12 Union Road, Cambridge, CB2 1EZ, UK (fax: +44-1223-336033; e-mail: deposit@ccdc.cam.ac.uk or www: http://www.ccdc.cam.ac.uk).

Acknowledgements

This work was supported by an ARC Large Grant (KSM), a Sir J. McNeil postgraduate scholarship (D.J.P.) and an ARC Fellowship (S.R.B.).

References

[1] T.G. Carrell, A.M. Tyryshkin, G.C. Dismukes, J. Biol. Inorg. Chem. 7 (2002) 2.
[2] M. Yagi, M. Kaneko, Chem. Rev. 101 (2001) 21.
[3] G. Aromi, M.W. Wemple, S.J. Aubin, K. Folting, D.N. Hendrickson, G. Christou, J. Am. Chem. Soc. 120 (1998) 5850.
[4] S. Wang, H.-L. Tsai, E. Libby, K. Folting, W.E. Streib, D.N. Hendrickson, G. Christou, Inorg. Chem. 35 (1996) 7578.
[5] J. Messinger, J.H. Robblee, U. Bergmann, C. Fernandez, P. G latzel, H. Visser, R.M. Cinco, K.L. McFarlane, E. Bellacchio, S.A. Pizarro, S.P. Cramer, K. Sauer, M.P. Klein, V.K. Yachandra, J. Am. Chem. Soc. 123 (2001) 7804.
[6] J.H. Robblee, J. Messinger, R.M. Cinco, K.L. McFarlane, C. Fernandez, S.A. Pizarro, K. Sauer, V.K. Yachandra, J. Am. Chem. Soc. 124 (2002) 7459.
[7] T. Lis, Acta Crystallogr., Sect. B 36 (1980) 2042.
[8] M. Soler, P. Artus, K. Folting, J.C. Huffman, D.N. Hendrickson, G. Christou, Inorg. Chem. 40 (2001) 4902.
[9] Y. Miyazaki, A. Bhattacharjee, M. Nakano, K. Saito, S.M.J. Aubin, H.J. Eppley, G. Christou, D.N. Hendrickson, M. Sorai, Inorg. Chem. 40 (2001) 6632.
[10] T. Kuroda-Sowa, M. Lam, A.L. Rheingold, C. Frommen, W.M. Reiff, M. Nakano, J. Yoo, A.L. Maniero, L.-C. Brunel, G. Christou, D.N. Hendrickson, Inorg. Chem. 40 (2001) 6469.
[11] S. Aubin, M.J.Z. Sun, H.J. Eppley, E. Rumberger, I.A. Guezei, K. Folting, A.L. Rheingold, G. Christou, D.N. Hendrickson, Polyhedron 20 (2001) 1139.
[12] P. Artus, C. Boskovic, J. Yoo, W.E. Streib, L.-C. Brunel, D.N. Hendrickson, G. Christou, Inorg. Chem. 40 (2001) 4199.
[13] B. Barbara, L. Thomas, F. Lionti, I. Chiorescu, A. Sulpice, J. Magn. Magn. Mater. 200 (1999) 167.
[14] W. Wernsdorfer, N. Aliaga-Alcalde, D.N. Hendrickson, G. Christou, Nature 416 (2002) 406.
[15] S.M.J. Aubin, N.R. Dilley, L. Pardi, J. Krzystek, M.W. Wemple, L.-C. Brunel, M.B. Maple, G. Christou, D.N. Hendrickson, J. Am. Chem. Soc. 120 (1998) 4991.
[16] S.M.J. Aubin, M.W. Wemple, D.M. Adams, H.-L. Tsai, G. Christou, D.N. Hendrickson, J. Am. Chem. Soc. 118 (1996) 7746.
[17] J. Yoo, E.K. Brechin, A. Yamaguchi, M. Nakano, J.C. Huffman, A.L. Maniero, L.-C. Brunel, K. Awaga, H. Ishimoto, G. Christou, D.N. Hendrickson, Inorg. Chem. 39 (2000) 3615.
[18] J. Yoo, A. Yamaguchi, M. Nakano, J. Krzystek, W.E. Streib, L.-C. Brunel, H. Ishimoto, G. Christou, D.N. Hendrickson, Inorg. Chem. 40 (2001) 4604.
[19] A.-L. Barra, B. Fabio, A. Caneschi, D. Gatteschi, C. Paulsen, C. Sangregorio, R. Sessoli, L. Sorace, Chem. Phys. Chem. 2 (2001) 523.
[20] Y. Pontillon, A. Caneschi, D. Gatteschi, R. Sessoli, E. Ressouche, J. Schweizer, E. Lelievre-Berna, J. Am. Chem. Soc. 121 (1999) 5342.
[21] A.L. Barra, D. Gatteschi, R. Sessoli, Chem. Eur. J. 6 (2000) 1608.
[22] A. Caneschi, D. Gatteschi, C. Sangregorio, R. Sessoli, A. Sorace, A. Cornia, M.A. Novak, C. Paulsen, W. Wernsdorfer, J. Magn. Magn. Mater. 200 (1999) 182.
[23] S.L. Castro, Z. Sun, C.M. Grant, J.C. Bollinger, D.N. Hendrickson, G. Christou, J. Am. Chem. Soc. 120 (1998) 2365.
[24] C. Cadiou, M. Murrie, C. Paulsen, V. Villar, W. Wernsdorfer, R.E.P. Winpenny, J. Chem. Soc., Chem. Commun. (2001) 2666.
[25] J.J. Sokol, A.G. Hee, J.R. Long, J. Am. Chem. Soc. 124 (2002) 7656.
[26] S.R. Batten, P. Jensen, C.J. Kepert, M. Kurmoo, B. Moubaraki, K.S. Murray, D.J. Price, J. Chem. Soc., Dalton Trans. (1999) 2987.
[27] D.J. Price, S.R. Batten, B. Moubaraki, K.S. Murray, J. Chem. Soc., Chem. Commun. (2002) 762.
[28] G. Longo, Gazz. Chim. Ital. 61 (1931) 575.
[29] Z. Otwinowski, W. Minor, Methods Enzymol. 276 (1997) 307.
[30] G.M. Sheldrick, SHELX-97, Program for Crystal Structure Refinement, University of Göttingen, Göttingen, Germany, 1997.
[31] B.J. Kennedy, K.S. Murray, Inorg. Chem. 24 (1985) 1552.
[32] M. Hvastijová, J. Kohout, J.W. Buchler, R. Boca, J. Kozísek, L. Jäger, Coord. Chem. Rev. 175 (1998) 17.
[33] M. Dunaj-Jurco, D. Miklos, L. Potocnak, L. Jäger, Acta Crystallogr., Sect. C 54 (1998) 1763.
[34] M. Hvastijová, J. Kohout, J. Kozísek, I. Svoboda, J. Coord. Chem. 47 (1999) 573.
[35] J.W. Buchler, M. Hvastijová, J. Kohout, J. Kozísek, Transition Met. Chem. 23 (1998) 215.

[36] D.J. Price, S.R. Batten, B. Moubaraki, K.S. Murray, unpublished results.
[37] N. Arulsamy, D.S. Bohle, J. Org. Chem. 65 (2000) 1139.
[38] F. Birkelbach, T. Weyhermuller, M. Lengen, M. Gerdan, A.X. Trautwein, K. Wieghardt, P. Chaudhuri, J. Chem. Soc., Dalton Trans. (1997) 4529.
[39] F. Birkelbach, U. Floerke, H.-J. Haupt, C. Butzlaff, A.X. Trautwein, K. Wieghardt, P. Chaudhuri, Inorg. Chem. 37 (1998) 2000.
[40] X. Li, D.P. Kessissoglou, M.L. Kirk, C.J. Bender, V.L. Pecoraro, Inorg. Chem. 27 (1988) 1.
[41] K.S. Murray, Adv. Inorg. Chem. 43 (1995) 261.
[42] J.B. Vincent, C. Christmas, H.R. Chang, Q. Li, P.D.W. Boyd, J.C. Huffman, D.N. Hendrickson, G. Christou, J. Am. Chem. Soc. 111 (1989) 2086.
[43] H.H. Thorp, J.E. Sarneski, R.J. Kulawiec, G.W. Brudvig, R.H. Crabtree, G.C. Papaefthymiou, Inorg. Chem. 30 (1991) 1153.